JGR Space Physics

RESEARCH ARTICLE
10.1029/2018JA026116

Special Section:
The Earth's Magnetosphere: New Tools, New Thinking, New Results

Oscillatory Flows in the Magnetotail Plasma Sheet: Cluster Observations of the Distribution Function

A. De Spiegeleer[1], M. Hamrin[1], H. Gunell[1,2], M. Volwerk[3], L. Andersson[4], T. Karlsson[3,5], T. Pitkänen[1,6], C. G. Mouikis[7], H. Nilsson[8], and L. M. Kistler[7]

[1]Department of Physics, Umeå University, Umeå, Sweden, [2]Belgian Institute for Space Aeronomy, Brussels, Belgium, [3]Space Research Institute, Austrian Academy of Sciences, Graz, Austria, [4]Laboratory for Atmospheric and Space Physics, University of Colorado Boulder, Boulder, CO, USA, [5]Space and Plasma Physics, School of Electrical Engineering, KTH Royal Institute of Technology, Stockholm, Sweden, [6]Shandong Provincial Key Laboratory of Optical Astronomy and Solar-Terrestrial Environment, Institute of Space Sciences, Shandong University, Weihai, China, [7]Department of Physics, University of New Hampshire, Durham, NH, USA, [8]Swedish Institute of Space Physics, Kiruna, Sweden

Abstract Plasma dynamics in Earth's magnetotail is often studied using moments of the distribution function, which results in losing information on the kinetic properties of the plasma. To better understand oscillatory flows observed in the midtail plasma sheet, we investigate two events, one in each hemisphere, in the transition region between the central plasma sheet and the lobes using the 2-D ion distribution function from the Cluster 4 spacecraft. In this case study, the oscillatory flows are a manifestation of repeated ion flux enhancements with pitch angle changing from 0° to 180° in the Northern Hemisphere and from 180° to 0° in the Southern Hemisphere. Similar pitch angle signatures are observed seven times in about 80 min for the Southern Hemisphere event and three times in about 80 min for the Northern Hemisphere event. The ion flux enhancements observed for both events are slightly shifted in time between different energy channels, indicating a possible time-of-flight effect from which we estimate that the source of particle is located ~ 5–25R_E and ~ 40–107R_E tailward of the spacecraft for the Southern and Northern Hemisphere event, respectively. Using a test particle simulation, we obtain ~21–46 R_E for the Southern Hemisphere event and tailward of $X \sim -65R_E$ (outside the validity region of the model) for the Northern Hemisphere event. We discuss possible sources that could cause the enhancements of ion flux.

Key Points:
- Oscillatory flows can be due to repeated particle flux enhancements with clear pitch angle patterns
- The pitch angle of the flux enhancements changes from 0 to 180 degrees in the Northern Hemisphere and from 180 to 0 degrees in the Southern Hemisphere
- The particles associated with the flux enhancements originate from a source tailward of the spacecraft

Correspondence to:
A. De Spiegeleer,
alexandre.de.spiegeleer@umu.se

Citation:
De Spiegeleer, A., Hamrin, M., Gunell, H., Volwerk, M., Andersson, L., Karlsson, T., et al. (2019). Oscillatory flows in the magnetotail plasma sheet: Cluster observations of the distribution function. *Journal of Geophysical Research: Space Physics*, *124*, 2736–2754. https://doi.org/10.1029/2018JA026116

Received 19 SEP 2018
Accepted 31 MAR 2019
Accepted article online 5 APR 2019
Published online 18 APR 2019

1. Introduction

The magnetotail plasma sheet hosts a plethora of phenomena. High-speed flows have naturally attracted a lot of attention due to their contributions to about 60% of the plasma transport while they are only observed for ~10% of the probing time (Angelopoulos et al., 1994). During the 90% of the time for which high-speed flows are not observed, other types of flows occur, and each of them should be studied to understand the magnetotail dynamics. These flows can be related to low-frequency waves (e.g., Zheng et al., 2006), flow vortices at the flanks of high-speed flows (e.g., Keiling et al., 2009), particle beams in the plasma sheet boundary layer (e.g., Takahashi & Hones Jr. 1988), and so forth. In particular, in this article, we focus on oscillatory flows in the magnetotail plasma sheet, which are oscillations in the velocity moments (e.g. De Spiegeleer et al., 2017; Panov et al., 2013).

Studies of the plasma flows in Earth's magnetotail often use moments of the distribution function while the distribution function provides more information. For example, analyzing the distribution function allows to distinguish between the high-speed flows observed in the central plasma sheet (CPS) and those observed in the plasma sheet boundary layer (e.g., Keiling et al., 2006; Raj et al., 2002). Therefore, to better understand oscillatory flows, we focus on studying the distribution function of oscillatory flows rather than the moments of the distribution function.

We use 2-D distribution functions from the Cluster 4 (C4) spacecraft to investigate two oscillatory flow events observed in the midtail outer CPS (Baumjohann et al., 1989), one in each hemisphere. Specifically, we observe, in association with the oscillatory flows, several nearly continuous changes with time of the pitch angles of oxygen ions, O^+, either from 0° (parallel to the magnetic field) to 180° (antiparallel to the magnetic field) or from 180° to 0° depending on the hemisphere (see sketch in Figures 1a and 1b).

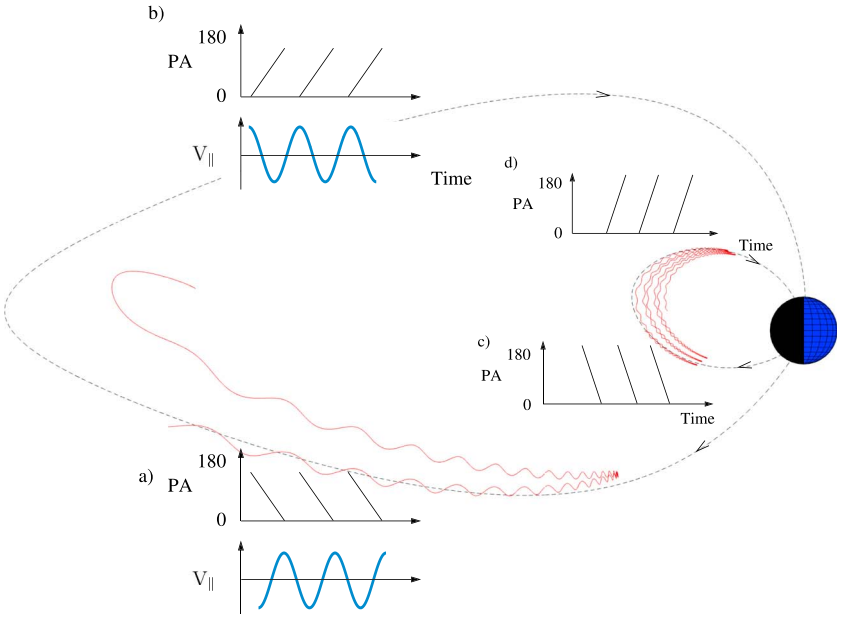

Figure 1. Sketch of one nearly dipolar and one stretched nightside field line (dashed) and two test particle trajectories (red). Sketch of the enhanced differential particle flux in the Southern Hemisphere (a and c) and the Northern Hemisphere (b and d) for the stretched (a and b) and dipolar (c and d) magnetic field line. PA = Pitch Angle.

To our knowledge, such pitch angle signatures have not attracted much attention in the literature. There exist only few observations made by, for example, Yang et al. (2011) and Ren et al. (2016; see also Ren et al., 2015, 2017, and references therein) in the inner magnetosphere on rather dipolar field lines (Figures 1c and 1d). According to Yang et al. (2011), the signatures could be the result of a combination of the time-of-flight effect and the drift-bounce resonance (where particles drift azimuthally and bounce between the Northern and Southern Hemispheres and are in resonance with a standing wave; Southwood & Kivelson, 1981, 1982). Because those are the only observations of the pitch angle signatures aforementioned, we introduce the work by Yang et al. (2011) but only to provide an interpretation of the pitch angle signatures. The mechanism responsible for the signatures in the magnetotail is, however, probably different than drift-bounce resonance.

According to Yang et al. (2011), the energization of particles via the drift-bounce resonance would cause an enhancement of particle flux in a certain energy range. The periodicity of the enhancement would be related to the wave period and the continuous change with time of the observed pitch angle would be caused by the time-of-flight effect of particles as they move away from the equatorial plane, over the spacecraft to their mirror points and back to the spacecraft. The time a particle takes to move along the field line can be evaluated by integrating $1/v_{\|}$ over the particle's trajectory, where $v_{\|}$ is the speed along the magnetic field line. Using the approximation provided by Baumjohann and Treumann (1997) for a magnetic dipole configuration gives times that are in agreement with the qualitative description provided by Yang et al. (2011), which is as follows. Consider particles with same kinetic energy but different equatorial pitch angle. A spacecraft off the equatorial plane, say in the Southern Hemisphere, would first observe the most antiparallel particles with 180° pitch angle and only later the particles with pitch angle closer to 90° because they have smaller field-aligned speed. The particles continue to move along the field-line beyond the spacecraft position until they reach their mirror points where they move back toward the spacecraft. Then, the first particles to be observed by the spacecraft are the ones with pitch angle close to 90°, as their mirror point is closer to the spacecraft. Particles with pitch angle closer to 0° are observed later, as they have longer distance to travel. This can explain the continuous pitch angle change from 180° to 0° in the Southern Hemisphere. Similar reasoning explains the 0° to 180° signature in the Northern Hemisphere. Because the time needed for the particles to move along the field line depends on $v_{\|}$ and therefore on the magnetic field configuration, the time dependences of the pitch angle (Figures 1a–1d) would typically differ between the inner magnetosphere (larger slope, Figures 1c and 1d) and the magnetotail (smaller slope, Figures 1a and 1b). Note that

the sketches are only indicative. In practice, it depends on the magnetic field line configuration and on the particles' energy.

Note that the pitch angle signatures reported by Yang et al. (2011) and Ren et al. (2016) were observed in the inner magnetosphere where the drift-bounce energization mechanisms is viable. As will be shown in this paper, our observations from the midtail plasma sheet where the magnetic field lines are stretched cannot easily be explained by the same mechanism. Yet, even if the mechanism causing the flux enhancement presented in this article is not the drift-bounce resonance, the time-of-flight interpretation by Yang et al. (2011) may still hold in Earth's magnetotail; that is, the particles are first observed as they propagate earthward from a source in the tail, they are then reflected at their mirror points, and they are observed again by the spacecraft as they move tailward.

In this article, we start by introducing the data and the instruments (section 2) and continue by presenting observations of an oscillatory flow event from the Southern Hemisphere for which the particle flux enhancement changes pitch angle from 180° to 0° (section 3.1). We evaluate the distance between the spacecraft and the source of particles using the energy-dispersed structures of the particle flux enhancements. Then, we present an oscillatory flow event from the Northern Hemisphere for which the particle flux changes pitch angle from 0° to 180° (section 3.2). Again, we evaluate the distance to the source using energy-dispersed structures. From the measured data we suggest that the source of particles is located tailward of the spacecraft, and to better investigate the source for both events, we use a test particle simulation (section 4). Finally, we discuss a number of possible energization mechanisms, which, together with a time-of-flight effect, may give rise to the observed pitch angle signatures (section 5).

2. Data and Instruments

This investigation is based on H^+ and O^+ data from the Cluster Ion Spectrometry-Composition Distribution Function) instrument (Rème et al., 2001) and magnetic field data from the FluxGate Magnetometer instrument (Balogh et al., 2001) on-board the C4 satellite (Escoubet et al., 2001). From the Cluster Ion Spectrometry-Composition Distribution Function instrument, we use the one-dimensional differential energy flux data (1-D energy-time spectrograms) and the data of the differential particle flux as a function of the energy and the pitch angle (energy-time spectrogram at constant pitch angle and pitch angle-time spectrogram at constant energy).

In addition, the high-resolution AL-index (Davis & Sugiura, 1966) data and the 1-min OMNI solar wind data (https://omniweb.gsfc.nasa.gov/) are used. Throughout the article, all vectorial quantities are expressed in the Geocentric Solar Ecliptic coordinate system.

3. Observations

In the following, we present two events, one in each hemisphere. The Southern Hemisphere event (section 3.1) occurred on 29 August 2003 from 20:40 UTC until 22:00 UTC and was observed in situ by C4. The Northern Hemisphere event (section 3.2) was also observed in situ by C4 and occurred on 28 August 2002 from 03:00 UTC until 04:25 UTC.

3.1. Southern Hemisphere

The AL-index, the negative of which is indicative of the magnitude of the westward auroral electrojet, and the Z component of the interplanetary magnetic field (IMF B_z) propagated to the nominal bow shock nose are shown in Figure 2 for the 17:10–23:00 UTC time interval on 29 August 2003. The event observed in situ by C4 extends from 20:40 to 22:00 UTC and is marked with a thick black line in Figure 2a. During that time interval, the westward auroral electrojet was declining, corresponding to the recovery phase of a substorm. Prior to the event, the IMF B_z was dominantly negative except during a 25-min interval (~19:50–20:15 UTC). The solar wind velocity in the X direction was about −560 km/s (not shown). The Kp index during the event was 3− but was 5 between 18:00 and 21:00 UTC.

In Figure 3, we show C4 data from 20:00 to 22:30 UTC on 29 August 2003. Figures 3a and 3b show the 1-D energy-time spectrogram for H^+ and O^+, respectively. Figures 3c and 3d show the pitch angle-time spectrogram for H^+ at 10.5 keV (instrumental energy range of 9.0–11.2 keV) and O^+ at 27.7 keV (23.7–30.2 keV), respectively. In Figures 3e–3g, we present the velocity moment data for O^+ in the X, Y, and Z direction, respectively. The red lines indicate the velocity components after low-pass filtering. The three components

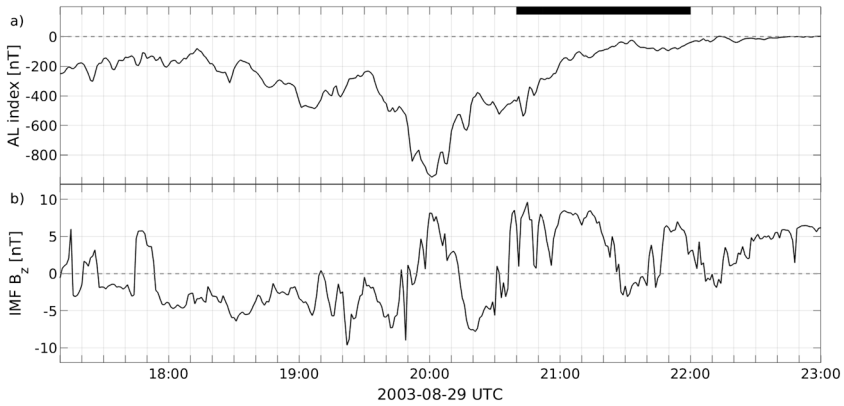

Figure 2. Data from 29 August 2003 of (a) the AL-index and (b) interplanetary magnetic field (IMF) B_z, which is shifted to the nominal bow shock nose.

of the velocity moments of H^+ are shown in Figure 3h. Finally, Figures 3i and 3j show the magnetic field data, B, and the plasma β computed using the proton data.

The event extends from 20:40 to 22:00 UTC, and it is selected because of the observed oscillations in the X and Y components of the O^+ velocity. Some oscillations can also be observed in H^+ velocity (Figure 3h). During the event, C4 was located at $\sim[-19, -1, -3]R_E$, below the neutral sheet as indicated by $B_x < 0$ (Figure 3i). Also, we notice that the magnitude of B_y and B_z was small compared to B_x, indicating that the tail was in a relatively stretched configuration. The magnitude of the magnetic field was between ~20 and ~30 nT, meaning that the spacecraft was close to the southern lobe. The entrance from the southern lobe into the plasma sheet at 20:08 UTC can easily be seen from the increase in the differential energy flux (Figures 3a and 3b). While entering the plasma sheet, C4 recorded fast H^+ ions with maximum velocity [1,549, 109.2, −182] km/s at 20:12:37 UTC. These high-speed H^+ are due to antiparallel (pitch angle larger than 90°) flux enhancements (Figure 3c) from which we deduce that the high-speed H^+ are earthward beams in the plasma sheet boundary layed (PSBL). Following Baumjohann et al. (1989), a value of $\beta < 1$ ($\beta > 1$) would indicate the outer (inner) CPS. From Figure 3j, we observe that during the event, β was below 1 with several short peaks above 1, suggesting that C4 was mostly in the outer CPS with several short excursions into the inner CPS.

Focusing on the 20:40–20:50 time interval, from Figures 3b and 3d we see that the spacecraft registered an enhancement in the O^+ flux associated with the pitch angle continuously changing from about 180° to 0°. Since the spacecraft was located below the neutral sheet, it first observed earthward and then tailward going O^+ (Figure 1a). A continuous or nearly continuous flux enhancement signature with pitch angle changing from ~180° to ~0° or from ~0° to ~180° will hereafter be referred to as a "Pitch Angle Slope Structure" (PASS). PASSs are observed repeatedly every ~10 min during the entire event (20:40–22:00) from the 10.5-keV energy channel up to the highest energy channel of the instrument, 35.2 keV (data not shown). The relatively periodic occurrences of PASS result in oscillations in the O^+ velocity moments (Figures 3e–3g), which may contribute to some of the oscillatory flows reported by De Spiegeleer et al. (2017).

In Figures 4c–4f, we present the energy-time spectrograms of O^+ at constant pitch angles (39°, 73°, 107°, and 152°). We observe a number of O^+ energy dispersed structures (flux enhancements decrease in energy as time increases) during the event (20:40–22:00). Note that they are best seen during 20:40–21:20 and for earthward ions (107° and 152° pitch angle). Energy dispersed structures are still observed at 73° pitch angle but are hardly seen for particles with 39° pitch angle. This may be due to the presence of the cold O^+ outflow beam (Figure 4c) that is superimposed on the population of interest. Or it may be that lower energetic particles, when moving tailward after mirroring, do not come back near the spacecraft location due to drifts perpendicular to the magnetic field.

One possible reason for energy dispersed signatures is the time-of-flight effect (see, e.g., Sharma et al., 2008). The dispersion of particles occurs whenever the particles have different velocities along the field line. This can be used to estimate the distance the particles cover along the magnetic field line (e.g., Sauvaud & Kovrazhkin, 2004). For this purpose, we use the energy dispersed data (Figure 4g) in a $1/v_{\parallel}$–time

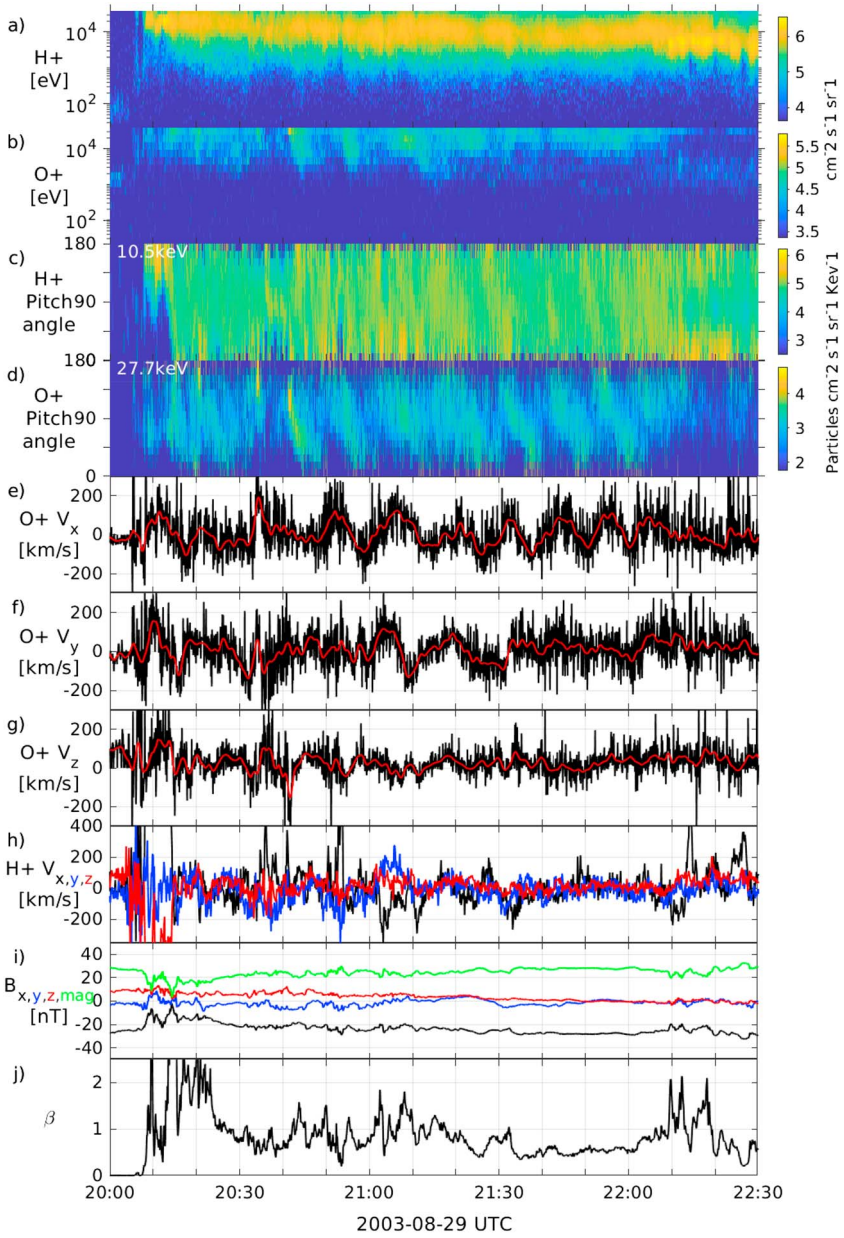

Figure 3. Cluster 4 data from 29 August 2003. (a and b) One-dimensional differential energy flux (1-D energy-time spectrogram) for H^+ and O^+. (c and d) Differential particle flux of H^+ at 10.5 keV and O^+ at 27.7 keV as a function of the pitch angle (pitch angle-time spectrogram). (e–g) O^+ velocity moments (black) and low-pass filtered data (red). (h) H^+ velocity moments. (i) Magnetic field components and magnitude. (j) Plasma β computed from the H^+ data.

spectrogram (Figure 4f) with $v_{\parallel}$ the speed along the magnetic field of O^+ with 152° pitch angle. Though oversimplifying, we assume that only the time-of-flight effect is responsible for the time dependence of the flux enhancements and also assume that the magnetic field is constant and no forces act on the particles between their source region (where the particles are initial accelerated) and the spacecraft. This is a zeroth-order approximation, which means that the method does not take into account the acceleration of particles between the source and the spacecraft due to the interaction with a shock or a wave (though these interactions certainly affect the particles' motion) nor does it take into account the distance traveled by the particles due to the convection of the field lines. We do not think that the magnetic field convection effect is significant. The typical convection speed in the plasma sheet is <100 km/s (Juusola et al., 2011), which is significantly smaller than the slowest particles used for evaluating the distance to the source (~330 km/s, 10.5 keV, and 152° pitch angle). Hence, the particles' distance covered due to the convection is expected to

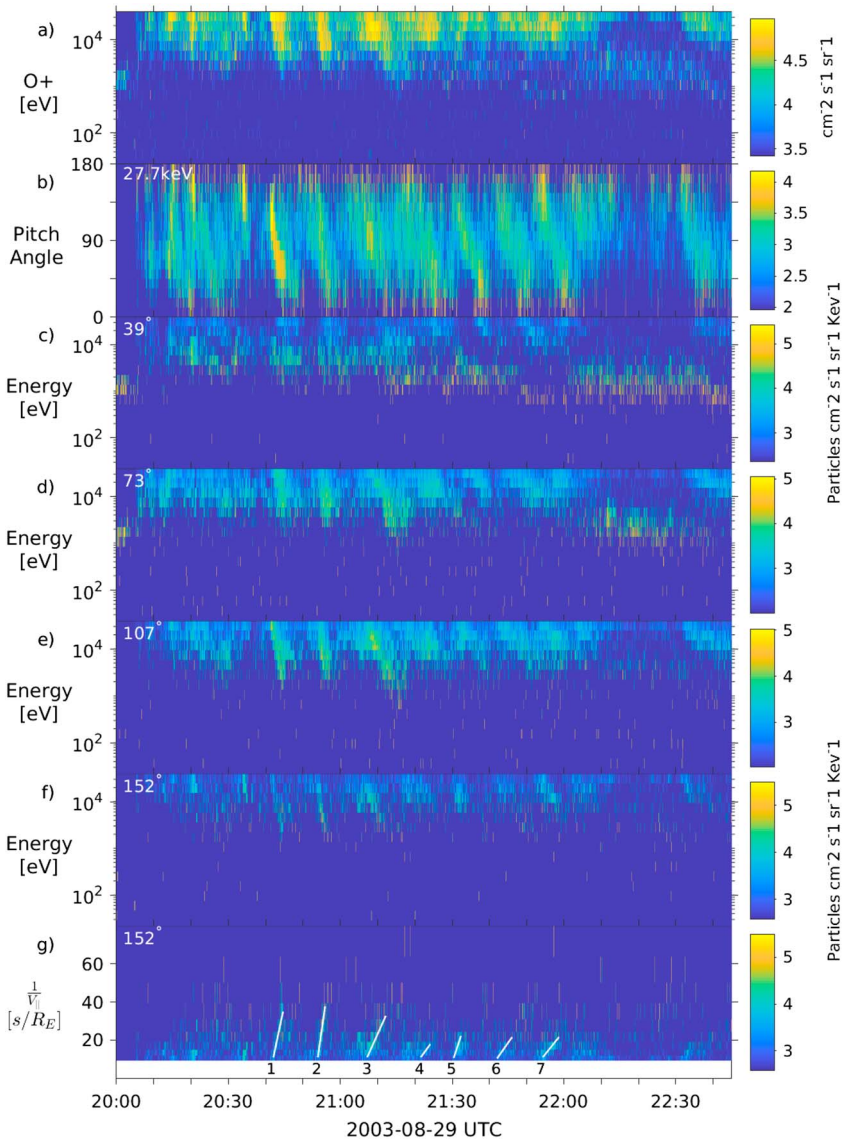

Figure 4. (a and b) Same as in Figures 3b and 3d, respectively. (c–f) Differential particle flux as a function of the energy for particles with 39°, 73°, 107°, and 152° pitch angle. (g) Same as (f) but shown as a function of the inverse parallel velocity rather than the energy. The energy dispersed structures are marked from 1 to 7.

be significantly smaller than the distance traveled along the field line under average convection conditions. During more active times, fast convections contribute significantly to the distance moved by the particles and estimates of the distance to the source using simple time-of-flight assumption would then be erroneous.

For each energy dispersed structure with 152° pitch angle, we fit 20 times the structure in the $1/v_{\parallel}$-time spectrogram by clicking on the beginning and ending points in the $1/v_{\parallel}$-time space. The resulting median of the 20 fits for each energy dispersed structure are shown as white lines in Figure 4g. This angle has been chosen for two main reasons. First, the particle flux is high enough to observe the energy-dispersed structures. Second, these particles have a high parallel velocity, implying that it took them a small amount of time to propagate from the source to the spacecraft and they therefore had only a short time to be affected by external forces and by the magnetic field convection.

The results from the linear fit can be found in Table 1. We find that the distance traveled by the particles to produce the observed energy-dispersed structure varies between 5 and 25 R_E. We interpret this distance as the distance along the field line between the spacecraft and the source of the particles when the particles were emitted. Because the spacecraft is at $\sim[-19, -1, -3]$ R_E and we are observing the stretched tail, the

Table 1
Beginning and Ending Time of the ED Structures From Figure 4g and the Corresponding Distances Covered by the Particles

	Begin	End	Distance (R_E)
ED 1	20:42:05	20:44:40	6.3
			7.0
			7.8
ED 2	20:54:01	20:55:57	3.8
			4.9
			5.4
ED 3	21:07:14	21:12:13	13.8
			15.0
			16.0
ED 4	21:21:34	21:24:09	18.3
			23.6
			25.6
ED 5	21:30:26	21:32:22	7.3
			9.7
			10.6
ED 6	21:42:02	21:46:04	17.8
			20.1
			23.6
ED 7	21:54:17	21:58:38	21.1
			23.6
			25.8

Note. ED = energy dispersed. For each ED, we show the 25th (top), 50th (middle), and 75th (bottom) percentiles.

source would be somewhere between $X \sim -24R_E$ and $X \sim -44R_E$. From the large variation in position estimate of the source, we suggest that either a single source retreats tailward or that there exists several sources.

Up till now, we have only discussed O^+ while three H^+ PASSs can also be observed in Figure 3c between 21:25 and 21:50. The visible H^+ PASSs are in the 4- to 13.4-keV energy range (not shown) while O^+ PASSs are observed at higher energies (10.5–35.2 keV). Note that H^+ PASSs are more difficult to resolve than O^+ PASSs, probably because of the denser background population, which is superimposed on the PASS particles. Also, no energy-dispersed structures are clearly observed for H^+. If such structures were observed, we could have again evaluated the distance to the source and compared it to the estimates obtained from the O^+ energy dispersed structures.

Comparing Figures 3c and 3d, we note that H^+ PASSs have steeper slopes than O^+ PASSs. Also, within a single species, the slopes of PASS slightly changes from one energy channel to the next (data not shown). These changes in slopes can be explained by the time-of-flight effect.

The slopes of PASS in the pitch angle-time spectrogram, if due to the time-of-flight effect, are directly related to the speed of the particles, not to the energy of the particles or the species. This can be understood by considering two particles of a species with the same energy, that is, same speed, v, but different pitch angles, α and β. The time difference between their observations after traveling a distance x is given by $\Delta t = \frac{x}{v}\left(\frac{1}{\cos\alpha} - \frac{1}{\cos\beta}\right)$. This shows that the slopes of PASS directly depends on the speed and that PASS from energy channels associated with different speeds should have different slopes.

3.2. Northern Hemisphere

In Figure 5, we present the AL-index and the IMF for an event observed in the Northern Hemisphere on 28 August 2002. The event observed in situ by C4 extends from 03:00 to 04:25 UTC and is marked with a

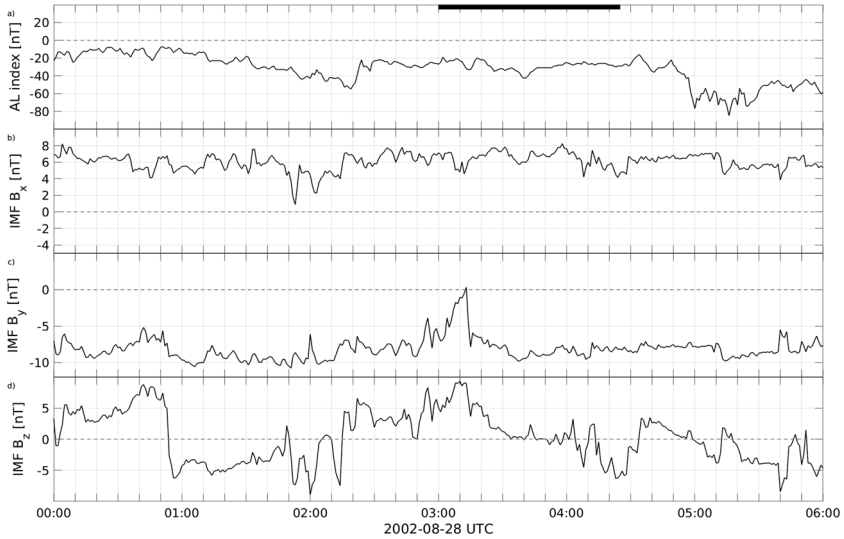

Figure 5. Data from 28 August 2002 of (a) the AL-index and (b–d) interplanetary magnetic field (IMF) B_x, B_y, and B_z, which are shifted to the nominal bow shock nose.

thick black line in Figure 5a. Contrary to the event in the Southern Hemisphere, the AL-index (Figure 5a) was relatively constant. It had an average of −29 nT, therefore indicating a low level of geomagnetic activity. Supporting the low geomagnetic activity is the low Kp index, 2−. The IMF B_z (Figure 5d) became positive about 40 min prior to the event and gradually decreased during the event. At the end of the event, IMF $B_z \sim -5$ nT. Note that IMF $B_x > 0$ and IMF $B_y < 0$ for an extended period of time. The solar wind velocity in the X direction was about −415 km/s.

In Figure 6, we present C4 observations from 28 August 2002, when the spacecraft was located at ∼[-18, -4, 3] R_E. The event starts at about 03:00 UTC and ends at 04:25 UTC. During that time, oscillations of O^+ velocity in the X direction can be observed. From the H^+ and O^+ flux increase at 02:40 UTC in the energy-time spectrogram (Figures 6a–b) and the magnetic field data (Figure 6g), we note that the spacecraft was in the northern lobe or really close to it. This is also supported by the plasma β value, which is mostly below 1 (not shown). Also, characteristics of the lobes are the outflow beams of oxygen that can be seen during the entirety of the time interval (Figure 6a) as the particles with energies below ∼2 keV.

The pitch angle-time spectrogram of O^+ at 27.7 keV is shown in Figure 6c. A clear PASS can be seen around 04:20 UTC (between 04:15 and 04:25 UTC). We will refer to it as "PASS A." A second possible PASS, "PASS B," which is broader, can be seen around 03:07 UTC (between ∼03:03 and 03:11 UTC). And a third possible PASS, "PASS C," which is even fainter and broader, occurred at ∼03:28 UTC (∼03:22–03:34 UTC). In contrast to the Southern Hemisphere event, the differential particle flux at 27.7 keV varies from ∼0° to 180° pitch angle in the Northern Hemisphere. This implies, similarly to the Southern Hemisphere event, that the enhancement first consists of earthward-moving and then tailward-moving particles.

We further analyze PASS A from Figure 6c by showing the pitch angle-time spectrogram (Figures 7a–7c) in three different energy channels (35.2, 21.7, and 13.4 keV) such that we cover parts of the energy range in which PASS A is present. We note that PASS A occurs later in lower-energy channels. Note also that PASS A becomes more diffuse and faint at lower energies until it can barely be observed at 6.5 keV (not shown). This time dependence between energy channels henceforth results in an energy-dispersed structure in the energy-time spectrograms. For example, we show in Figure 7d the energy-time spectrogram at 28° pitch angle. Similarly to the energy-dispersed structure observed in the Northern Hemisphere, we do 20 linear fits in the $1/v_{||}$-time spectrogram (Figure 7e) to estimate the distance of the source of particles. The median result is shown in Figure 7e (white line). From the 20 fits, we obtained that the median distance to the source from the spacecraft is 107 R_E; the 25th and 75th percentiles are 99 and 118R_E, respectively.

The particle flux of PASS B becomes higher and sharper at lower energies (Figures 7b and 7c). PASS B shows much less time dependence between energy channels compared to PASS A. This indicates that the source is located much closer than at the time when PASS A is observed. From this energy dispersed structure, we

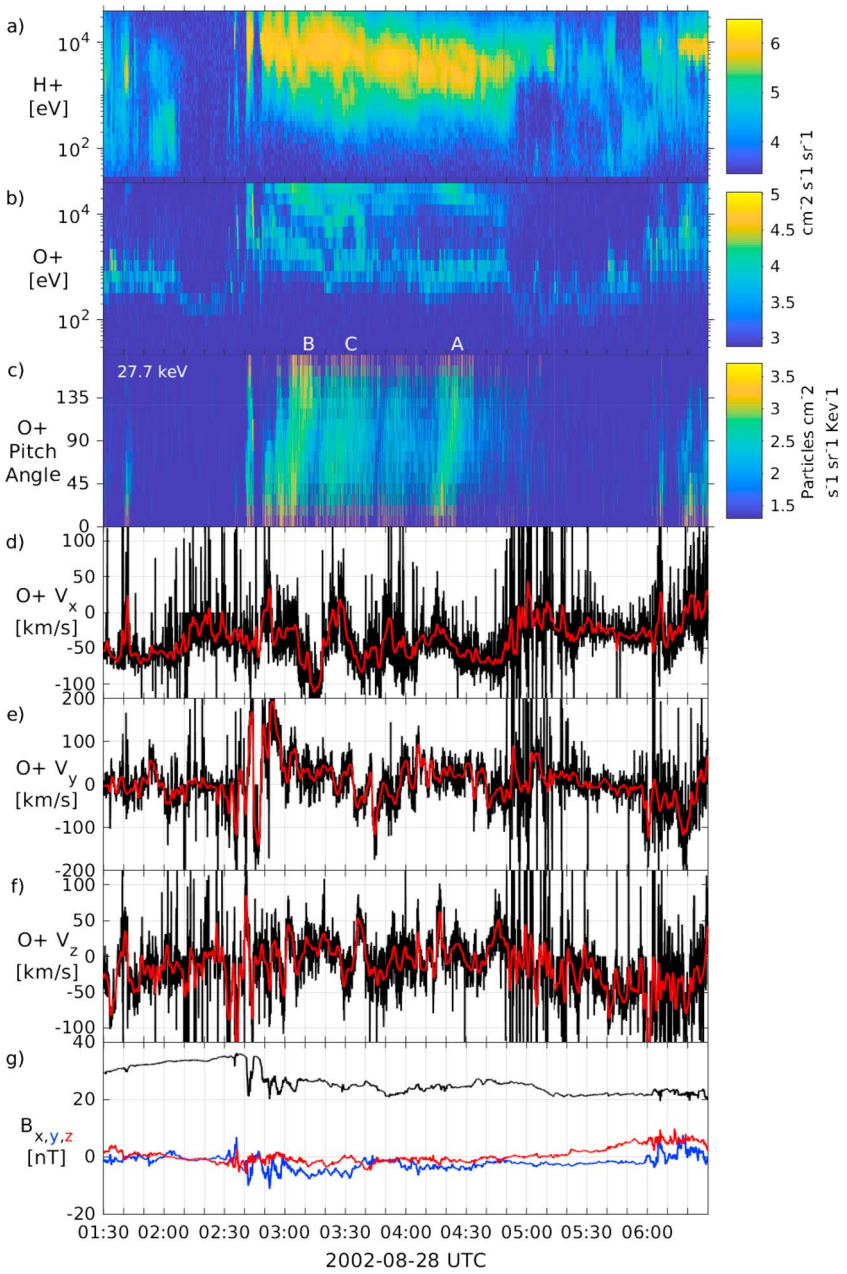

Figure 6. Cluster 4 data from 28 August 2002. (a and b) H^+ and O^+ energy-time spectrogram. (c) Pitch angle-time spectrogram for O^+ at 27.7 keV. (d–f) O^+ velocity moments (black) and low-pass filtered data (red). (g) Magnetic field data.

obtain (again doing 20 linear fits in Figure 7e) that the median distance to the source is ~40 R_E and the 25th and 75th percentiles are 37 and 42 R_E, respectively. Note that the estimated distance to the source obtained from PASS A and PASS B changes by ~60 R_E in about 1h20. PASS C, similarly to PASS B, becomes sharper and has higher particle flux in lower-energy channels. However, PASS C does not show energy-dispersed signatures, and no estimates of the source distance can be made using the simple time-of-flight method. That PASS B and PASS C signatures become clearer in certain energy channels probably result from the following. First, there are less background particles, and second, the source of PASS particles produces more particles in certain energy channels. These PASSs likely account for the O^+ oscillatory flows observed in the X direction (Figure 6d). From the distance to the source obtained from PASS A and PASS B, we suggest (similarly to the Southern Hemisphere event) that either the source retreated tailward or there exist several

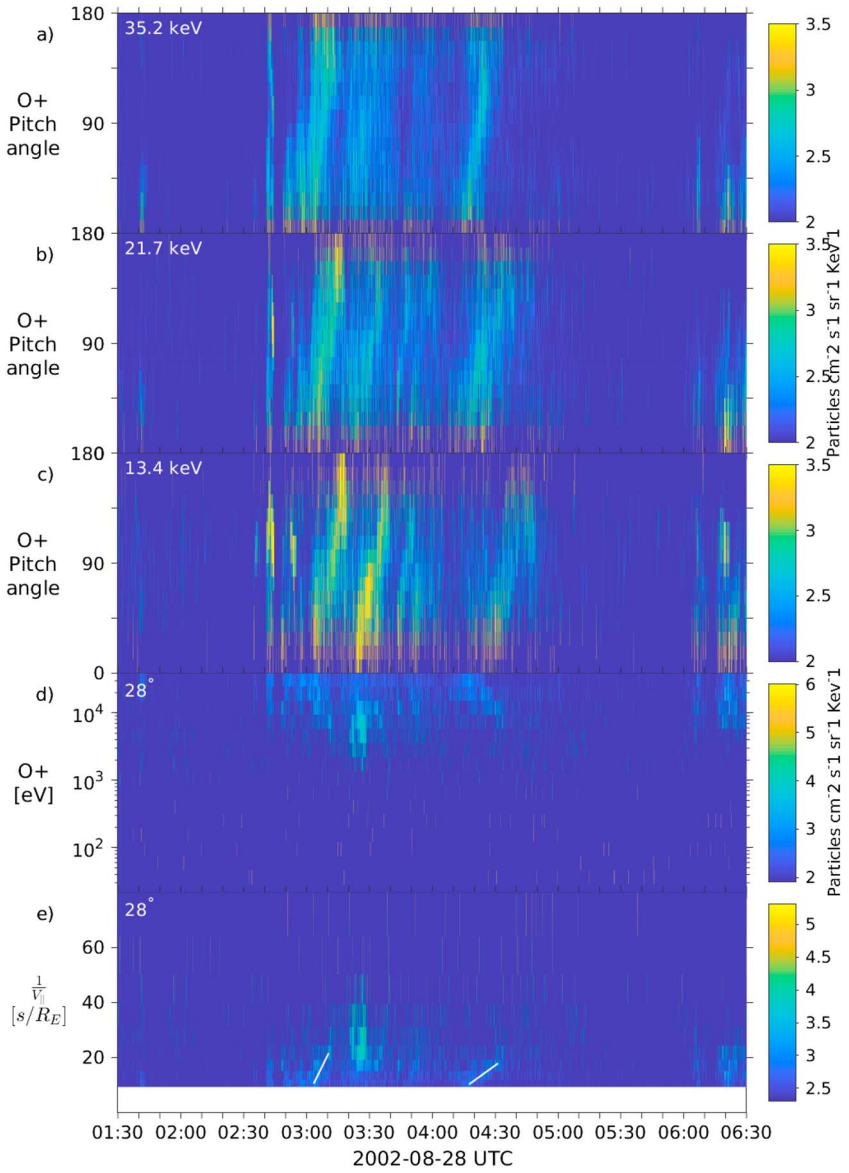

Figure 7. (a–c) O^+ pitch angle-time spectrogram at 35.2, 21.7, and 13.4 keV. (d) Energy-time spectrogram of O^+ particles with 28° pitch angle. (e) Same as (d) but shown as a function of the inverse parallel velocity rather than the energy.

sources tailward of the spacecraft. For this event, we do not observe clear H^+ PASS nor energy dispersed structures, and we have therefore omitted to show the data.

4. Test Particle Simulation

We trace test particles in a model magnetosphere to improve the understanding of the observations from section 3 and to estimate the location of the source(s) of PASS particles for both events. The simulation uses Tsyganenko 96 (Tsyganenko, 1995) and Weimer (Weimer, 2001) models for the magnetic and electric field, respectively. We trace the particles both forward and backward in time. By tracing the particles backward in time, that is, before they reached the spacecraft, we may gain information on the size and location of the source. And by tracing the trajectory of the particles forward in time, that is, after being detected by the spacecraft, we can investigate the future of the particles and whether or not they may be the particles observed moving tailward after mirroring. As the input data for the models, we use the solar wind data

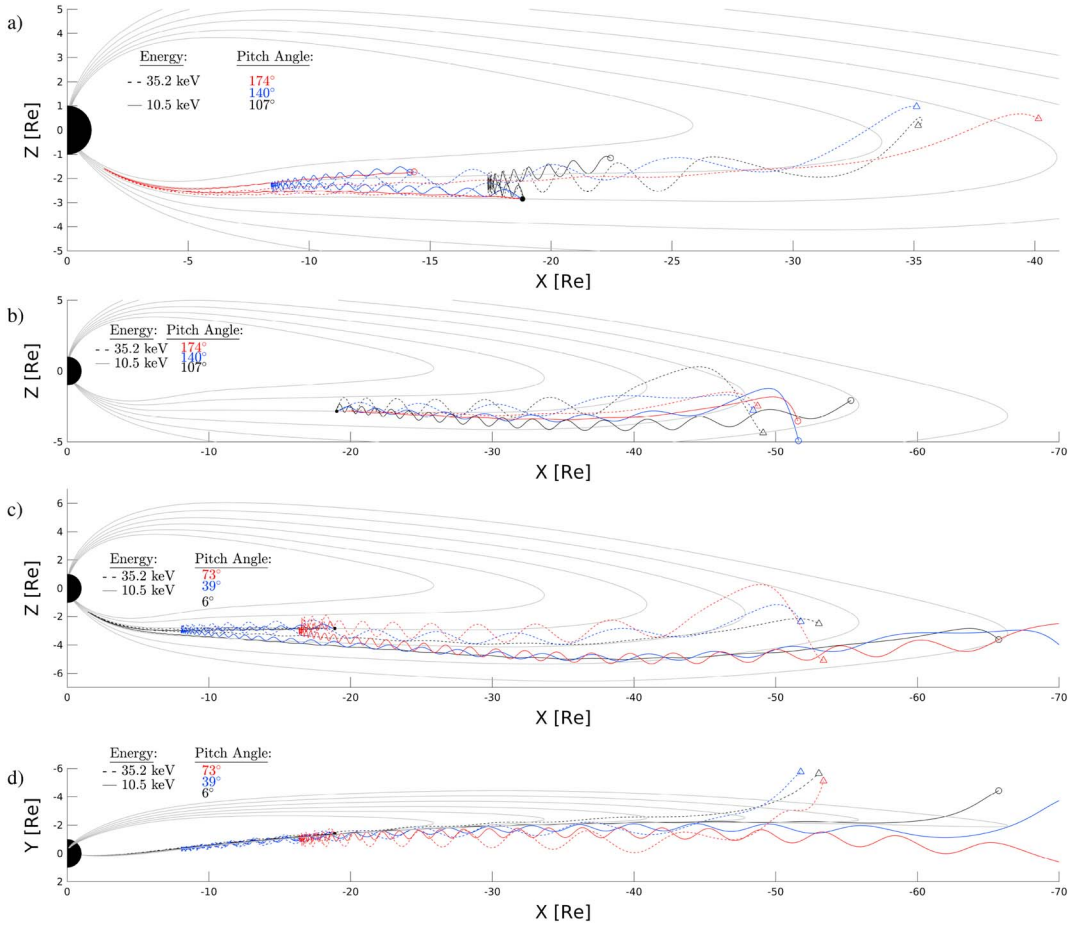

Figure 8. Test particle tracing for input data on 29 August 2003, 21:00 UTC. The particles are launched from the small black circle (spacecraft). The trajectories are shown with dashed lines for the 35.2-keV particles (triangles as end points) and solid lines for the 10.5-keV particles (circles as end points). (a) Trajectory of earthward-moving particles for 10 min after their detection. (b) Trajectory of earthward-moving particles for 20 min before their detection. (c and d) Trajectory of tailward-moving particles for 40 min in the *xz*-plane and *xy*-plane before their detection.

shifted to the nominal bow shock nose from 29 August 2003 21:00 UTC for the Southern Hemisphere event and from 28 August 2002 04:20 UTC for the Northern Hemisphere event.

4.1. Southern Hemisphere

In sections 1 and 3, we interpreted the tailward-moving particles as the reflected particles initially moving earthward. Hence, we neglected all drifts even though they may be important. In Figure 8a, we show the trajectories of six earthward-moving O^+ (initial pitch angles 174°, 140°, and 107°) at the extreme energies for which PASS are observed (10.5 and 35.2 keV). The particles are launched from the location of C4 at 21:00 UTC (small black circle), and the selected pitch angles for the simulation simply correspond to some of C4 instrumental channels for which enhancements of the differential O^+ flux are observed. The characteristic timescale of PASS is about 10 min, and we therefore show the particles' trajectories for that duration. The position of the particles after 10 min are marked using circles for the 10.5-keV particles and triangles for the 35.2-keV particles.

We observe in Figure 8a that the particles with same pitch angle but different energies have similar trajectories but the lower energetic particles drift slightly more toward the equator before reaching their mirror point. The trajectories are similar simply because the local pitch angle, ϕ, depends on the local magnetic field, B, following $\sin^2\phi = \frac{B}{B_0}\sin^2\phi_0$ (where the subscript 0 corresponds to a reference position) and not on the energy. The difference in the equatorward drift is due to the ExB-drift affecting more the lower energetic particles as they take longer to reach their mirror points.

We find that because of the ExB-drift, most particles drift equatorward by about 1 R_E or more before coming back anywhere close to the spacecraft. Note that during those 10 min, the spacecraft moved by ∼[0.002, 0.041, −0.096] R_E, which is negligible compared to the particle motion. That the particles drift equatorward by about 1 R_E means that the particles never return exactly to the spacecraft and that the tailward-moving particles must originate from higher latitude field lines. Therefore, the size of the region near the spacecraft for which the particles forming PASS can be observed has to be relatively wide (at least one or two R_E in Z).

To investigate the source, we follow the trajectory of the particles before they reached the spacecraft. We show in Figure 8b the trajectories (20 min) of six earthward-moving particles (10.5 and 35.2 keV and three pitch angles) before they were detected. We observe a latitudinal separation between the 35.2- and 10.5-keV particles. The lowest energetic particles are seen closest to the southern lobe. From these trajectories and assuming that the source is near or at the neutral sheet, we suggest that the detected particles come from a widespread region along X between −55 and $-40R_E$ (between 21 and $36R_E$ tailward of the spacecraft). This result roughly agrees with the time-of-flight estimates (Figure 7e; Table 1). From the trajectories shown in Figure 8b, the particles detected by the spacecraft with low energies seem to be emitted from a region tailward of the more energetic particles.

Note that the source probably extends even farther than approximately $-55R_E$. This is because, as aforementioned, the tailward-moving particles observed by the spacecraft have drifted equatorward even more than the earthward going particles. Therefore, we show the trajectories (40 min) of six tailward-moving O^+ (10.5 and 35.2 keV and three pitch angles) before they reached the spacecraft (Figure 8c). We again observe a clear separation in Z between the particles with different energies. We note however that the particles with same energies but different pitch angles have remarkably similar trajectories apart from the position of the mirror points. The trajectories shown in Figure 8c would indicate that the source could extend down to $X \sim -65R_E$ ($46R_E$ tailward of the spacecraft). From the trajectories shown in Figures 8b and 8c, several interpretations concerning the source can be made. The source may either be spatially large (∼20 R_E), there may be several sources along X, or there may be a single localized source moving in the X direction.

Concerning the size of the source in the Y direction, we show in Figure 8d the trajectories in the XY plane of the 8 tailward-moving O^+ at 10.5 and 32.5 keV before reaching the spacecraft. Ignoring the large gyroradius of O^+ when the particles move close to the neutral sheet, the particles are not spread much in Y, and the source may be in the $-3R_E \leq Y \leq 0R_E$ range. This seems to be almost independent of the particles' energy.

4.2. Northern Hemisphere

The Northern Hemisphere event occurred during quieter magnetospheric conditions than the Southern Hemisphere event (Figures 2, 3, 5, and 6) and the distance to the source obtained from simple time-of-flight estimates is significantly larger. We investigate the shape of PASS in the pitch angle-time spectrogram. Also, we investigate the source position by considering the particles' trajectories before their detection by C4.

To investigate the shape of PASS and whether or not the tailward-moving particles can be interpreted as the initially earthward-moving particles, we simulate earthward-moving particles and see when they come back near the spacecraft. In particular, we study PASS A (Figure 6c) at 35.2 keV. We show PASS A in Figure 9a, and its outline is shown using black stars. The outline is obtained by identifying the maxima of the smoothed differential particle flux for each pitch angle range. The time in Figure 9a is shifted such that the maximum of the 6° pitch angle channel is at time 0. In our simulation, we launch the earthward-moving particles from the spacecraft position with the time delay between them obtained from the outline of PASS A shown in Figure 9a. For simplicity, we only show the trajectories of three initially earthward-moving particles (Figure 9b) and show the time along the particles' trajectory using a gray scale. The 6° particle is launched at time 0 min, the 39° particle at time 1.73 min, and the 73° particle at time 4.47 min. These particles come back near the spacecraft with a pitch angle of ∼174°, 141°, and 107° (∼180°—initial pitch angle) at time 6.2, 6.9, and 7.3 min, respectively. The times at which the particles come back near the spacecraft (as close as possible in the xz-plane) after mirroring are indicated using white stars in Figure 9a.

Some small deviations are observed between the simulation results and the actual data measured by C4, but the general trend obtained from the simulation and the data follow each other remarkably well considering the simplicity of the model. The only significant difference between the simulation and the PASS outline is observed for the largest pitch angle channel (174°), but we note that the differential particle flux is very low

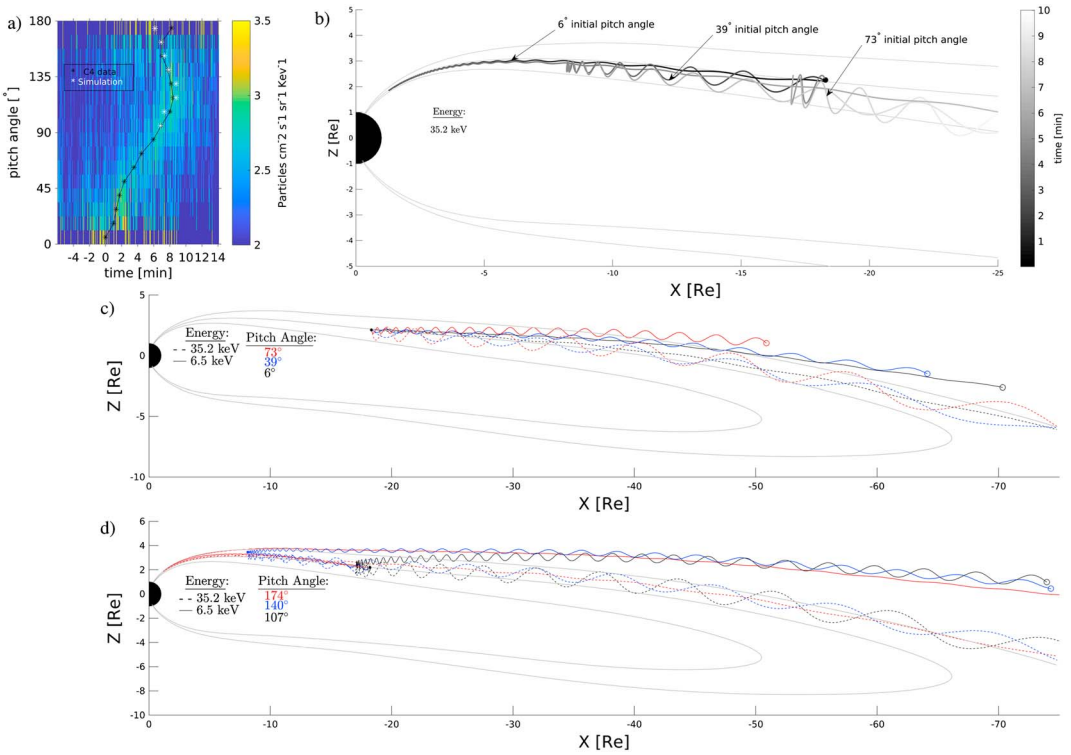

Figure 9. Test particle tracing on August 28 2002, 04:20 UTC. The particles are launched from the small black circle (spacecraft). The trajectory of particles with 35.2-keV energy is shown with dashed lines (triangles as end points), and those with an energy of 6.5 keV are shown with solid lines (circles as end points). (a) PASS A (Figure 7a) and the maximal differential particle fluxes (black stars) as a function of the pitch angle and time since the maximum at 6° pitch angle. (b) Trajectory of earthward-moving particles after their detection by the spacecraft. The particles with 6°, 39°, and 73° pitch angles are launched at time 0, 1.73, and 4.47 min, respectively. The gray scale indicates the time since the launch of the 6° particle. (c) Trajectory of earthward-moving particles for 20 min before their detection. (d) Trajectory of tailward-moving particles for 40 min before their detection.

and it is not clear if the maximum indicated by the black star is representative of the PASS. These results confirm that we can interpret the tailward-moving particles as the initially earthward-moving particles.

We investigate the position of the source in a similar fashion to the approach used for the Southern Hemisphere event (Figures 8b and 8c). We trace backward in time a total of 12 particles, 6 detected as earthward moving (Figure 9c) and 6 as tailward moving (Figure 9d). The six earthward-moving (Figure 9c) particles (35.2 and 6.5 keV and three pitch angles) are traced backward for 20 min while the six tailward-moving (Figure 9d) particles are traced backward for 40 min. Similarly to the Southern Hemisphere event, a separation between the particles appear depending on the particles' energies with the lowest energetic originating from a region mapping closer to the northern lobe. Assuming that the source is near the neutral sheet, the simulation would indicate that the source is located far downtail, outside the region in which the Tsyganenko model is valid. Nevertheless, it seems that the source is located in the distant tail. This is in agreement with the results obtained from the time-of-flight estimates (Figure 7e), which suggested the source to be $\sim 107 R_E$ tailward of the spacecraft.

5. Discussion

The Southern Hemisphere event occurs after observing plasma with speeds above 1,500 km/s, which suggests that the observations are done during active plasma sheet conditions. It is thus possible that the magnetic moment (first adiabatic invariant) of O^+ particles is not conserved. Indeed, the gyroradius of a 27.7 keV O^+ particle with 90° pitch angle in a 25-nT magnetic field is ~3,800 km and its gyroperiod is ~42 s. However, our interpretation that the time dependence of PASS results from the time-of-flight effect does not require that the particles' magnetic moment is exactly conserved but only that the particles' motion roughly consist of the gyration around the field lines and that the particles move along the magnetic field line. Minor

changes to the typical particle motion will not significantly change the shape of PASS. However, if the particles were to be significantly accelerated by a shock, a wave, a dipolarization front, and so forth, our estimates of the distance to the source using the time-of-flight effect would be invalid. Such acceleration would give rise to nonlinearities in the $1/v_{||}$-time spectrogram (Figures 4g and 7e). These are not clearly observed.

If PASS are indeed due to the time-of-flight effect and if the particles are simply gyrating and moving along their field lines, the shape of PASS must depend on the geometry of the magnetic field between the source and the spacecraft for the first half of the PASS. Similarly, it should depend on the magnetic configuration between the spacecraft and the particles' mirror points for the second half of the PASS. In a static magnetic field configuration of the magnetosphere, we would expect that each PASS are similar. However, the PASSs observed in the Southern Hemisphere (Figure 3) are not all exactly the same, nor is it the case for the Northern Hemisphere event (Figure 6). We therefore suggest that the changes with time of the shape of PASS are due to a time dependency of the magnetic configuration of the magnetosphere.

In theory, PASS signatures combined with time-of-flight calculations could be used to evaluate the distance to the source. However, the particles' pitch angle evolve as the particles move along the field line due the variations in the magnetic field magnitude. The changes in pitch angle result in variations in the field-aligned speed of the particles. Thus, to calculate accurately the distance to the source using the time of flight, one needs informations of the fields along the particle trajectories. Therefore, in practice, it is not possible to estimate accurately the distance between the spacecraft and the source from the PASS signatures alone.

Up till now, we have assumed that PASS result from particles launched/accelerated at the source with a broad range of pitch angles and that they are not affected by any acceleration mechanism between the source and where the particles are observed. The particles move from the source to the spacecraft and the pitch angles change due to variations in the magnetic field strength. An alternative scenario that can also result in the apparition of a large range of pitch angles may be as follows. Assume that the source emits particles that are only nearly parallel or antiparallel in a broad energy range. If the magnetic field magnitude does not increase significantly before the particles reach the spacecraft, no particles would be observed with pitch angle close to 90°. However, if we assume that a mechanism energizes the particles in the perpendicular direction, the initially field-aligned particles get an increase of their total energy and of their pitch angle, therefore becoming more perpendicular but keeping the same field-aligned speed. The particles with pitch angles close to 90° at the spacecraft might thus initially have been emitted as field-aligned particles. They would arrive after the first PASS particles because their initial speed along the magnetic field has been conserved.

The observation of consecutive enhanced differential particle fluxes from the Southern and Northern Hemispheres (Figures 3-6) and the tracing of the particles (Figures 8 and 9) point toward the existence of a time-dependent source tailward of the spacecraft modulating the differential particle flux. In the following sections, we discuss a number of mechanisms known to cause enhancements of O^+ flux via an energization of particles or an increase of the particles density, or both. When possible, the mechanisms are considered for the Southern Hemisphere event (Figure 3), as it has the longest and clearest signatures. Unfortunately, the spacecraft from the Cluster mission were the only ones in the magnetotail to record the event, and they were too close to one another to observe any differences in the data. No spacecraft from other missions were located tailward of C4 to possibly observe the source.

5.1. Wave-Particle Interactions

In the inner magnetosphere, the nearly dipolar magnetic field configuration is such that the particles bounce between the Northern and Southern Hemisphere and drift azimuthally. This allows for particles to interact with the electric field of a standing wave and possibly gain energy. The resonant interaction between a standing wave and drifting and bouncing particles is known as drift-bounce resonance or simply drift resonance depending on the specifics of the particles motion relative to the wave (Southwood & Kivelson, 1981, 1982). There exists several observations of such resonances in the inner magnetosphere (e.g., Claudepierre et al., 2013; Ren et al., 2017; Takahashi et al., 1990; Yang et al., 2011): Off the equatorial plane, the particle flux data show a pitch angle dependence similar to those presented in this article (e.g., Ren et al., 2016; Yang et al., 2011).

In this investigation, we present data from the magnetotail where the magnetic field is no longer dipolar and it is hence unclear if the drift-bounce or drift resonance is viable. To our knowledge, drift and drift-bounce resonances in the midtail have never been reported.

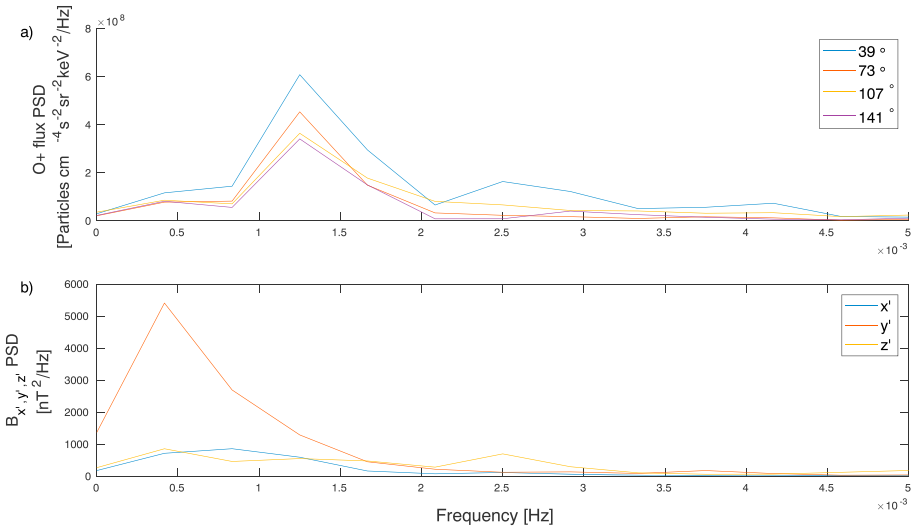

Figure 10. Normalized Welch power spectral density (PSD) estimates using 40-min window overlapping by 75% of (a) the differential particle flux of O^+ at 27.7 keV (as shown in Figure 3d) and of (b) the magnetic field. The colors in (a) correspond to four pitch angle values and those in (b) refer to the three directions of the magnetic field in field-aligned coordinate system.

The resonance requires a standing wave and particles interacting with it for several wave periods. Such standing wave may exist in the stretched tail as suggested by Zheng et al. (2006). They presented electric and magnetic field data from the midtail that were interpreted as a standing wave with 15-min wave period. The possible existence of standing waves in the midtail would indicate that resonances could be possible. However, our test particle simulation showed that particles are expected to drift by at least one Earth radius over approximately one wave period. During that time, the particles move into regions with different magnetic fields and plasma densities and thus different Alfvén speeds. Thus, as the particles drift, they enter regions of different wave frequencies. We therefore think it is unlikely for particles to interact resonantly with a standing wave in the midtail. Still, nonresonant energization of particles might occur.

To better assess the validity of the wave-particle interaction scenarios (resonant and nonresonant) for our first event (Figure 3), we investigate the wave activity in the magnetic field at the frequency associated with the repeated PASS. The power spectral densities computed from the differential particle flux of O^+ at 27.7 keV for four pitch angles and from the magnetic field on 29 August 2003, from 20:40 to 22:00, are shown in Figures 10a and 10b, respectively. The three components of the magnetic field and the associated power spectral densities are expressed in a coordinate system where z' is along the background magnetic field (30-min running average forward and backward in time), x' is perpendicular to z' and as earthward as possible, and y' completes the right-handed basis. Figure 10a indicates PASS wave power at about 1.25 mHz (~13.3 min) for the four pitch angles. The power spectral density estimate of the magnetic field data at the spacecraft location shows no clear peak near 1.25 mHz, and we therefore think that there is no wave at the spacecraft location that would be responsible for the repeated PASS. However, because the only available data are from the spacecraft position, we cannot eliminate the possibility that the PASS are due to wave-particle interaction tailward of Cluster.

5.2. Transient Ionospheric Outflow

Oxygen of ionospheric origin can be observed in the plasma sheet (e.g., Kronberg et al., 2014; Mukai et al., 1994), and, if the thermalization processes in the plasma sheet are slow enough, some properties of the ionospheric outflow of O^+ might still be observable in the plasma sheet. Interestingly, Nilsson et al. (2008) reported enhancements of O^+ flux at the polar caps with typical time scales of 5 to 10 min. This property might therefore still be present in the plasma sheet and might explain the repeated O^+ flux enhancements presented in this article. The outflowing O^+ observed at the polar cap is moving tailward, and, if the associated field line reconnects somewhere tailward, the O^+ might then be observed to propagate earthward in the hemisphere opposite to that from which they escaped the ionosphere. This could explain the origin of

the repeated enhancements of O^+, and the specific pitch angle signatures might again be explained by the time-of-flight effect of mirroring particles.

Because the particles would be emitted from the ionosphere and that, for this mechanism to be viable, reconnection needs to occur somewhere in the tail, the particles should propagate at least about the typical distance to the near-earth neutral line, which is between −16 and $-30R_E$ in X (Miyashita et al., 2009; Nagai et al., 1998). For our Southern Hemisphere event, the estimated propagation distances for the particles are between 5 and $25R_E$ (Table 1), which makes the first three energy dispersed structures (Figure 4) unlikely to be due to ionospheric outflow while the following structures might be. In addition, note that the Southern Hemisphere event was observed during a substorm recovery phase during which the near-earth neutral line is expected to retreat tailward (Baumjohann et al., 1999). We would thus expect even greater propagation distances than during conditions when a typical near-earth neutral line is present. Therefore, it is unclear if the Southern Hemisphere PASSs result from transient ionospheric outflow.

5.3. Neutral Sheet Resonances

Trapped particle motion in the neutral sheet is dominantly chaotic, and the particles are energized by the cross-tail electric field, E_y (Büchner & Zelenyi, 1989; Lyons & Speiser, 1982). They gain energy depending on E_y and on the magnetic field component normal to the neutral sheet, $B_n \approx B_z$. The energy gained decreases for increasing X due to the inverse B_n dependency. As highlighted by the simulation by Ashour-Abdalla et al. (1993) of mantle particles populating the plasma sheet, there are two peculiar particle trajectories for the particles after they have been accelerated in the neutral sheet. If they exit the neutral sheet field aligned, they are seen as beams in the PSBL. Such particles are energized at localized X positions along the neutral sheet (resonances) resulting in spatially separated beams in $|Z|$ with the most energetic ones observed at larger $|Z|$. These are known as "beamlets" (see Ashour-Abdalla et al., 1993, for the simulation and, e.g., Sauvaud & Kovrazhkin, 2004; Zelenyi et al., 2006 for observations). At other localized positions along the neutral sheet, the particles are energized and exit the neutral sheet but are not field aligned. In such case, the particles follow an orbit called "cucumber" and are trapped in the plasma sheet. These particles spend most of their time moving earthward and tailward, interacting several times with the neutral sheet.

Clearly, it is unlikely that our observations are beamlets for two main reasons. (1) Beamlets are observed at the transition between the lobes and the plasma sheet while our observations are more from the outer CPS than the PSBL. (2) Beamlets are collimated field-aligned particles. Because the particles are well field aligned, they are expected to mirror close to Earth and not close to a spacecraft that would be probing the midtail. Hence, no particles with pitch angle close to 90° should be observed if the observed events are beamlets events. We compared beamlets events using Cluster data (Grigorenko et al., 2007; Zelenyi et al., 2006) to the Northern and Southern Hemisphere events presented in this article and conclude that our observations are not beamlets.

On the other hand, the velocity distribution function where particles with "cucumber" trajectories are observed should have a large range of pitch angles but should lack the most field-aligned particles. The particles originating from a resonance have similar energies but are spread in pitch angle. Therefore, their parallel velocities are different, which results in a spatial spread due to the ExB-drift (as explained in section 4 and as can be seen from the simulation in Figure 8). Hence, a spacecraft moving into or out of the CPS should observe that the energy and the pitch angle depend on the spatial position of the spacecraft. For the inward motion in the Southern Hemisphere, the spacecraft should first observe pitch angle changing from 180° to 0° for the most energetic particles and then observe similar PASS but at lower energy. For the outward motion of the spacecraft in the Southern Hemisphere, the pitch angle should vary from 0° to 180°, and the energy associated with these consecutive PASS should increase.

For the Southern Hemisphere event (Figure 3), the spacecraft enters the plasma sheet from the southern lobe and moves later toward the southern lobe again. If the PASS particles are due to the neutral sheet resonances, two obvious signatures should be observed. First, the energy-time spectrogram should show a decrease in energy between PASS during the inward motion and an increase in energy during the outward motion. Second, the PASS should vary from 180° to 0° during the inward motion and from 0° to 180° during the outward motion of the spacecraft. However, we do not find any such signatures. This makes the neutral sheet resonances scenario unlikely to cause PASS.

5.4. Reconnection

Reconnection is known to energize particles in the magnetotail, which results in the appearance of high-speed bulk flows. One often distinguishes between field-aligned beams and convective high-speed flows. As their names suggest, field-aligned beams are particles moving parallel or antiparallel to the magnetic field, and they are often found in the boundary layer between the plasma sheet and the lobes. The convective high-speed flows are particles moving perpendicular to the magnetic field, and they are usually confined near the equatorial plane (e.g., Raj et al., 2002).

The PASS presented in this article are observed in the outer CPS, which is somewhat between the CPS, where convective high-speed flows are common, and the plasma sheet boundary layer, where field-aligned beams are common. Also, the distribution function associated with PASS is not purely field aligned nor is it purely perpendicular since the enhancement in the pitch angle-time spectrogram varies between 0° and 180°. It is therefore tempting to speculate that the particles forming PASS would also originate from reconnection. However, to our knowledge, no observations have ever shown that reconnection can be modulated at a ∼10-min period, which would be required to explain the repeated PASS. Simulations have shown that several reconnection locations can form in the plasma sheet and move earthward (e.g., Palmroth et al., 2017, and references therein), taking ∼1 min between the observation of different X-line at a fixed location (Palmroth et al., 2017), therefore providing a ∼1-min periodicity. Alternative solar wind input might change the characteristic time from ∼1 min to ∼10 min, which would then provide the right periodicity for PASS.

5.5. Dipolarization Fronts

Dipolarization fronts are characterized by a sharp increase in B_z and can be observed together with high-speed flows (e.g., Angelopoulos et al., 1992). A number of observations and simulations (e.g., Artemyev et al., 2012; Birn et al., 2015, 2017; Eastwood et al., 2015; Ukhorskiy et al., 2018; Zhou et al., 2012) have shown that particles are energized when interacting with a dipolarization front. In the equatorial plane, this results in the appearance of energized plasma some dozens of seconds before the observation of a dipolarization front. Zhou et al. (2012) observed precursor flows away from the equator some minutes before the observations of precursor flows in the equatorial plane and suggested that the particles energized by a dipolarization front may propagate toward higher latitudes.

If the particles energized at dipolarization fronts in the CPS can indeed make their way to the outer CPS, it could result in enhanced O^+ flux. However, explaining the repeated PASS would require a train of dipolarization fronts separated by about 10 min. To our knowledge, this has never been reported. An occurrence rate of 1 dipolarization front per 3.9 hr was calculated by Fu et al. (2012) by using 9 years of Cluster 1 data, therefore making it unlikely that PASS are caused by the interaction of particles and dipolarization fronts.

6. Summary and Conclusion

In this article, we present in situ data from the C4 spacecraft from the midtail plasma sheet for two oscillatory flow events, one in each hemisphere. The events are from the transition region between the CPS and the tail lobes. We observe that the oscillatory flows are associated with repeated ion flux enhancements in the pitch angle-time spectrograms. The enhancements change from 0° to 180° pitch angle in the Northern Hemisphere whereas it varies from 180° to 0° in the Southern Hemisphere.

For the Southern Hemisphere event, C4 observes enhancements of O^+ flux varying from 180° to 0° pitch angle every ∼13 min for about 80 min. These structures (PASS) are observed in the 10.5- to 35.2-keV energy range but with small time delays between the energy channels. Based on these energy dependences (energy-dispersed structures), we estimate from simple time-of-flight considerations that the source of PASS particles is between 5 and $25R_E$ tailward of the spacecraft (between -44 and $-24\,R_E$ in X) and that there are either several sources or a single source that retreats tailward with time. The results from the backward tracing of test particles simulation would indicate that the source is farther down tail, between -40 and $-65\,R_E$ in X with the lower energetic particles coming from farther down tail than the more energetic ones. For the Northern Hemisphere event, the O^+ flux enhancement is observed to vary from 0° to 180° pitch angle, three times in about 80 min. Two of the three PASS shows energy-dispersed structure from which we estimate that the source is between 40 and $107R_E$ tailward of the spacecraft. Using the test particle simulation, the source is in the far tail, outside the region of validity of the model. For both events, the pitch angle dependence of O^+ flux suggests a source located tailward of the spacecraft while the fact that PASSs are repeated several times indicates a time-dependent source.

We discuss several potential sources for the observed signatures but none of them seem to unarguably explain repeated PASS. To better understand the general properties of PASS and the source of PASS particles, a statistical study and multi-spacecraft studies should be conducted.

Acknowledgments
We thank the FGM and CIS teams as well as the Cluster Science Archive (CSA) for providing calibrated Cluster data. We also thank the World Data Center for Geomagnetism, Kyoto for the AL index data, and the Space Physics Data Facility (SPDF) for the OMNI solar wind data. All data can be accessed at https://www.cosmos.esa.int/web/csa, https://omniweb.gsfc.nasa.gov/. A. D. S. and M. H. acknowledge support by the grants from the Swedish National Space Board, projects 105/14 and 271/14.

References

Angelopoulos, V., Baumjohann, W., Kennel, C. F., Coroniti, F. V., Kivelson, M. G., Pellat, R., et al. (1992). Bursty bulk flows in the inner central plasma sheet. *Journal of Geophysical Research*, *97*(A4), 4027—4039. https://doi.org/10.1029/91JA02701

Angelopoulos, V., Kennel, C. F., Coroniti, F. V., Pellat, R., Kivelson, M. G., Walker, R. J., et al. (1994). Statistical characteristics of bursty bulk flow events. *Journal of Geophysical Research*, *99*(A11), 21,257–21,280. https://doi.org/10.1029/94JA01263

Artemyev, A. V., Lutsenko, V. N., & Petrukovich, A. A. (2012). Ion resonance acceleration by dipolarization fronts: Analytic theory and spacecraft observation. *Annales Geophysicae*, *30*(2), 317—324. https://doi.org/10.5194/angeo-30-317-2012

Ashour-Abdalla, M., Berchem, J. P., BÃijchner, J., & Zelenyi, L. M. (1993). Shaping of the magnetotail from the mantle: Global and local structuring. *Journal of Geophysical Research*, *98*(A4), 5651—5676. https://doi.org/10.1029/92JA01662

Balogh, A., Carr, C. M., Acuña, M. H., Dunlop, M. W., Beek, T. J., Brown, P., et al. (2001). The cluster magnetic field investigation: overview of in-flight performance and initial results. *Annales Geophysicae*, *19*(10/12), 1207—1217. https://doi.org/10.5194/angeo-19-1207-2001

Baumjohann, W., Hesse, M., Kokubun, S, Mukai, T., Nagai, T., & Petrukovich, A. A. (1999). Substorm dipolarization and recovery. *Journal of Geophysical Research*, *104*(A11), 24,995–25,000. https://doi.org/10.1029/1999JA900282

Baumjohann, W., Paschmann, G., & Cattell, C. A. (1989). Average plasma properties in the central plasma sheet. *Journal of Geophysical Research*, *94*(A6), 6597—6606. https://doi.org/10.1029/JA094iA06p06597

Baumjohann, W., & Treumann, R. A. (1997). *Basic space plasma physics*. London: Imperial College Press.

Birn, J., Chandler, M., Moore, T., & Runov, A. (2017). Ion velocity distributions in dipolarization events: Beams in the vicinity of the plasma sheet boundary. *Journal of Geophysical Research: Space Physics*, *122*, 8026—8036. https://doi.org/10.1002/2017JA024231

Birn, J., Hesse, M., Runov, A., & Zhou, X. (2015). Ion beams in the plasma sheet boundary layer. *Journal of Geophysical Research: Space Physics*, *120*, 7522—7535. https://doi.org/10.1002/2015JA021573

Büchner, J., & Zelenyi, L. M. (1989). Regular and chaotic charged particle motion in magnetotaillike field reversals: 1. Basic theory of trapped motion. *Journal of Geophysical Research*, *94*(A9), 11,821–11,842. https://doi.org/10.1029/JA094iA09p11821

Claudepierre, S. G., Mann, I. R., Takahashi, K., Fennell, J. F., Hudson, M. K., Blake, J. B., et al. (2013). Van allen probes observation of localized drift resonance between poloidal mode ultra-low frequency waves and 60 keV electrons. *Geophysical Research Letters*, *40*, 4491—4497. https://doi.org/10.1002/grl.50901

Davis, T. N., & Sugiura, M. (1966). Auroral electrojet activity index AE and its universal time variations. *Journal of Geophysical Research*, *71*(3), 785—801. https://doi.org/10.1029/JZ071i003p00785

De Spiegeleer, A., Hamrin, M., Pitkänen, T., Volwerk, M., Mann, I., Nilsson, H., et al. (2017). Low frequency oscillatory flow signatures and high-speed flows in the Earth's magnetotail. *Journal of Geophysical Research: Space Physics*, *122*, 7042—7056. https://doi.org/10.1002/2017JA024076

Eastwood, J. P., Goldman, M. V., Hietala, H., Newman, D. L., Mistry, R., & Lapenta, G. (2015). Ion reflection and acceleration near magnetotail dipolarization fronts associated with magnetic reconnection. *Journal of Geophysical Research: Space Physics*, *120*, 511—525. https://doi.org/10.1002/2014JA020516

Escoubet, C. P., Fehringer, M., & Goldstein, M. (2001). Introduction the cluster mission. *Annales Geophysicae*, *19*(10/12), 1197—1200. https://doi.org/10.5194/angeo-19-1197-2001

Fu, H. S., Khotyaintsev, Y. V., Vaivads, A., André, M., & Huang, S. Y. (2012). Occurrence rate of earthward-propagating dipolarization fronts. *Geophysical Research Letters*, *39*, L10101. https://doi.org/10.1029/2012GL051784

Grigorenko, E. E., Sauvaud, J.-A., & Zelenyi, L. M. (2007). Spatial-temporal characteristics of ion beamlets in the plasma sheet boundary layer of magnetotail. *Journal of Geophysical Research*, *112*, A05218. https://doi.org/10.1029/2006JA011986

Juusola, L., Østgaard, N., & Tanskanen, E. (2011). Statistics of plasma sheet convection. *Journal of Geophysical Research*, *116*, A08201. https://doi.org/10.1029/2011JA016479

Keiling, A., Angelopoulos, V., Runov, A., Weygand, J., Apatenkov, S. V., Mende, S., et al. (2009). Substorm current wedge driven by plasma flow vortices: Themis observations. *Journal of Geophysical Research*, *114*, A00C22. https://doi.org/10.1029/2009JA014114

Keiling, A., Parks, G. K., Rème, H., Dandouras, I., Wilber, M., Kistler, L., et al. (2006). Energy-dispersed ions in the plasma sheet boundary layer and associated phenomena: Ion heating, electron acceleration, Alfvén waves, broadband waves, perpendicular electric field spikes, and auroral emissions. *Annales Geophysicae*, *24*(10), 2685—2707. https://doi.org/10.5194/angeo-24-2685-2006

Kronberg, E. A., Ashour-Abdalla, M., Dandouras, I., Delcourt, D. C., Grigorenko, E. E., Kistler, L. M., et al. (2014). Circulation of heavy ions and their dynamical effects in the magnetosphere: Recent observations and models. *Space Science Reviews*, *184*(1), 173—235. https://doi.org/10.1007/s11214-014-0104-0

Lyons, L. R., & Speiser, T. W. (1982). Evidence for current sheet acceleration in the geomagnetic tail. *Journal of Geophysical Research*, *87*(A4), 2276—2286. https://doi.org/10.1029/JA087iA04p02276

Miyashita, Y., Machida, S., Kamide, Y., Nagata, D., Liou, K., Fujimoto, M., et al. (2009). A state of the art picture of substorm-associated evolution of the near-Earth magnetotail obtained from superposed epoch analysis. *Journal of Geophysical Research*, *114*, A01211. https://doi.org/10.1029/2008JA013225

Mukai, T., Hirahara, M., Machida, S., Saito, Y., Terasawa, T., & Nishida, A. (1994). Geotail observation of cold ion streams in the medium distance magnetotail lobe in the course of a substorm. *Geophysical Research Letters*, *21*(11), 1023—1026. https://doi.org/10.1029/93GL02424

Nagai, T., Fujimoto, M., Saito, Y., Machida, S., Terasawa, T., Nakamura, R., et al. (1998). Structure and dynamics of magnetic reconnection for substorm onsets with geotail observations. *Journal of Geophysical Research*, *103*(A3), 4419—4440. https://doi.org/10.1029/97JA02190

Nilsson, H., Waara, M., Marghitu, O., Yamauchi, M., Lundin, R., Rème, H., et al. (2008). Transients in oxygen outflow above the polar cap as observed by the cluster spacecraft. *Annales Geophysicae*, *26*(11), 3365—3373. https://doi.org/10.5194/angeo-26-3365-2008

Palmroth, M., Hoilijoki, S., Juusola, L., Pulkkinen, T. I., Hietala, H., Pfau-Kempf, Y., et al. (2017). Tail reconnection in the global magnetospheric context: Vlasiator first results. *Annales Geophysicae*, *35*(6), 1269—1274. https://doi.org/10.5194/angeo-35-1269-2017

Panov, E. V., Kubyshkina, M. V., Nakamura, R., Baumjohann, W., Angelopoulos, V., Sergeev, V. A., & Petrukovich, A. A. (2013). Oscillatory flow braking in the magnetotail: Themis statistics. *Geophysical Research Letters*, *40*, 2505—2510. https://doi.org/10.1002/grl.50407

Raj, A., Phan, T., Lin, R. P., & Angelopoulos, V. (2002). Wind survey of high-speed bulk flows and field-aligned beams in the near-Earth plasma sheet. *Journal of Geophysical Research*, *107*(A12), SMP 3–1–SMP 3—17. https://doi.org/10.1029/2001JA007547

Rème, H., Aoustin, C., Bosqued, J. M., Dandouras, I., Lavraud, B., Sauvaud, J. A., et al. (2001). First multispacecraft ion measurements in and near the Earth's magnetosphere with the identical cluster ion spectrometry (CIS) experiment. *Annales Geophysicae*, *19*(10/12), 1303—1354. https://doi.org/10.5194/angeo-19-1303-2001

Ren, J., Zong, Q. G., Wang, Y. F., & Zhou, X. Z. (2015). The interaction between ULF waves and thermal plasma ions at the plasmaspheric boundary layer during substorm activity. *Journal of Geophysical Research: Space Physics*, *120*, 1133—1143. https://doi.org/10.1002/2014JA020766

Ren, J., Zong, Q. G., Zhou, X. Z., Rankin, R., & Wang, Y. F. (2016). Interaction of ulf waves with different ion species: Pitch angle and phase space density implications. *Journal of Geophysical Research: Space Physics*, *121*, 9459—9472. https://doi.org/10.1002/2016JA022995

Ren, J., Zong, Q. G., Zhou, X. Z., Rankin, R., Wang, Y. F., Gu, S. J., & Zhu, Y. F. (2017). Phase relationship between ULF waves and drift-bounce resonant ions: A statistical study. *Journal of Geophysical Research: Space Physics*, *122*, 7087—7096. https://doi.org/10.1002/2016JA023848

Sauvaud, J.-A., & Kovrazhkin, R. A. (2004). Two types of energy-dispersed ion structures at the plasma sheet boundary. *Journal of Geophysical Research*, *109*, a12213. https://doi.org/10.1029/2003JA010333

Sharma, A. S., Nakamura, R., Runov, A., Grigorenko, E. E., Hasegawa, H., Hoshino, M., et al. (2008). Transient and localized processes in the magnetotail: A review. *Annales Geophysicae*, *26*(4), 955—1006. https://doi.org/10.5194/angeo-26-955-2008

Southwood, D. J., & Kivelson, M. G. (1981). Charged particle behavior in low-frequency geomagnetic pulsations 1. Transverse waves. *Journal of Geophysical Research*, *86*(A7), 5643—5655. https://doi.org/10.1029/JA086iA07p05643

Southwood, D. J., & Kivelson, M. G. (1982). Charged particle behavior in low-frequency geomagnetic pulsations, 2. Graphical approach. *Journal of Geophysical Research*, *87*(A3), 1707—1710. https://doi.org/10.1029/JA087iA03p01707

Takahashi, K., & Hones Jr., E. (1988). ISEE 1 and 2 observations of ion distributions at the plasma sheet-tail lobe boundary. *Journal of Geophysical Research*, *93*(A8), 8558—8582. https://doi.org/10.1029/JA093iA08p08558

Takahashi, K., McEntire, R. W., Lui, A. T. Y., & Potemra, T. A. (1990). Ion flux oscillations associated with a radially polarized transverse pc 5 magnetic pulsation. *Journal of Geophysical Research*, *95*(A4), 3717—3731. https://doi.org/10.1029/JA095iA04p03717

Tsyganenko, N. A. (1995). Modeling the earth's magnetospheric magnetic field confined within a realistic magnetopause. *Journal of Geophysical Research*, *100*(A4), 5599—5612. https://doi.org/10.1029/94JA03193

Ukhorskiy, A. Y., Sorathia, K. A., Merkin, V. G., Sitnov, M. I., Mitchell, D. G., & Gkioulidou, M. (2018). Ion trapping and acceleration at dipolarization fronts: High-resolution MHD and test-particle simulations. *Journal of Geophysical Research: Space Physics*, *123*, 5580–5589. https://doi.org/10.1029/2018JA025370

Weimer, D. R. (2001). An improved model of ionospheric electric potentials including substorm perturbations and application to the geospace environment modeling November 24, 1996, event. *Journal of Geophysical Research*, *106*(A1), 407—416. https://doi.org/10.1029/2000JA000604

Yang, B., Zong, Q.-G., Fu, S. Y., Takahashi, K., Li, X., Wang, Y. F., et al. (2011). Pitch angle evolutions of oxygen ions driven by storm time ULF poloidal standing waves. *Journal of Geophysical Research*, *116*, a03207. https://doi.org/10.1029/2010JA016047

Zelenyi, L. M., Grigorenko, E. E., Sauvaud, J.-A., & Maggiolo, R. (2006). Multiplet structure of acceleration processes in the distant magnetotail. *Geophysical Research Letters*, *33*, L06105. https://doi.org/10.1029/2005GL024901

Zheng, Y., Lui, A. T. Y., Mann, I. R., Takahashi, K., Watermann, J., Chen, S.-H., et al. (2006). Coordinated observation of field line resonance in the mid-tail. *Annales Geophysicae*, *24*(2), 707—723. https://doi.org/10.5194/angeo-24-707-2006

Zhou, X., Ge, Y. S., Angelopoulos, V., Runov, A., Liang, J., Xing, X., et al. (2012). Dipolarization fronts and associated auroral activities: 2. Acceleration of ions and their subsequent behavior. *Journal of Geophysical Research*, *117*, A10227. https://doi.org/10.1029/2012JA017677